Contemporary Physics
Publication details, including instructions for authors and subscription information:
http://www.tandfonline.com/loi/tcph20

# Design considerations for near-field enhancement in optical antennas

Roberto Fernández-García[a], Yannick Sonnefraud[a], Antonio I. Fernández-Domínguez[a], Vincenzo Giannini[a] & Stefan A. Maier[a]
[a] Imperial College London, Department of Physics, London SW7 2AZ, UK
Published online: 16 Jan 2014.

To cite this article: Roberto Fernández-García, Yannick Sonnefraud, Antonio I. Fernández-Domínguez, Vincenzo Giannini & Stefan A. Maier , Contemporary Physics (2014): Design considerations for near-field enhancement in optical antennas, Contemporary Physics, DOI: 10.1080/00107514.2013.850788

To link to this article: http://dx.doi.org/10.1080/00107514.2013.850788

*Contemporary Physics*, 2014
http://dx.doi.org/10.1080/00107514.2013.850788

Taylor & Francis
Taylor & Francis Group

# Design considerations for near-field enhancement in optical antennas

Roberto Fernández-García, Yannick Sonnefraud*, Antonio I. Fernández-Domínguez, Vincenzo Giannini and Stefan A. Maier

*Department of Physics, Imperial College London, London SW7 2AZ, UK*

(*Received 20 August 2013; accepted 29 September 2013*)

Nanoantennas for visible and infrared radiation can strongly enhance the interaction of light with matter by their ability to localise electromagnetic fields on nanometric scales. This allows for the engineering of the absorption and radiation capabilities of nanoemitters, such as dye molecules or quantum dots. In this article, we discuss the main parameters influencing the near-field enhancement provided by dimer-type nanoantennas, the configuration most thoroughly studied in the literature. To facilitate the design of structures, we analyse the influence of the substrate, adhesion layers and a reflective metal underlayer, as well as their arrangement in a periodic fashion. We also highlight the factors which increase the damping of the localised plasmonic modes and the spectral differences between far and near-field resonances.

**Keywords:** nanoantennas; localised surface plasmon resonances; cross-section; field enhancement



## 1. Introduction

In recent years, optical antennas [1–4] working in the visible to near-IR spectral regimes and based on localised surface plasmon resonances (LSPR) have been intensely studied for their many applications in the field of nanophotonics [5–11]. These devices are characterised by the ability to capture free-space electromagnetic radiation and focus it to a small region below the diffraction limit. In addition, they present scattering cross-sections several times larger than their physical area, which can be used to increase the interaction of any nano-object located in their vicinity with free space radiation at the LSPR frequency. The strong field enhancement provided by optical antennas is the source of well-known applications in the photonics technology, such as Surface-Enhanced Raman Scattering (SERS) [12,13], multiphoton absorption [14] and the modification of the properties of fluorescent emitters (dyes, quantum dots...) [7]. Apart from those applications, optical nanoantennas have been used more recently in a wide range of fields such as nanomedicine [15–17], photovoltaics [18], optical sensing [19] or photocatalysis [20].

This article presents a numerical study providing a compilation of some of the most relevant capabilities of nanoantennas, focusing on the parameters that experimentally would determine their optical properties, and including considerations to bear in mind in the fabrication process to optimise their performance. We discuss the influence on the field enhancement and scattering cross-section of the following factors: the type of metal, the adhesion layer, the substrate, and the use of periodic arrays. In addition, a special emphasis will be made on the effect of the antenna design on the spectral shift between near-field and far-field peak intensities [21–24]. This is of particular interest for applications that take advantage of the near-field response of nanoantennas (such as SERS or fluorescence enhancement), as the probing of their scattering properties is easily accessible experimentally, whereas accessing their near-field characteristics comprehensively remains a challenge.

Since general analytical solutions to Maxwell's equations do not exist, numerical methods are required to describe the optical properties of metal nanoparticles. The finite difference time domain (FDTD) method [25] provides numerical solutions of the time-dependent Maxwell equations, discretised by using central-difference approximations to space and time partial derivatives. The fundamentals of the FDTD approach were established in 1966 by K.S. Yee [26], who designed the space grid and time-stepping algorithm, which is the base of the method. The materials are modelled by specifying their characteristic permittivity and permeability at every grid point, usually in homogeneous regions, at whose interfaces proper continuity conditions are needed. In this time advancing algorithm, the fields at each time instant are obtained as a function of previous values in time. One of the most relevant features of the method is that by performing a single simulation in which a broadband pulse is used as the source, the FDTD method allows obtaining the response of the system over a wide range of frequencies. In addition, all the electromagnetic field components are obtained

*Corresponding author. Email: y.sonnefraud@imperial.ac.uk

directly. This fact provides high stability to the calculations and makes the technique very useful in plasmonics, where all the components of the electromagnetic field are relevant. The calculations presented in this article were performed using Lumerical FDTD Solutions,[1] a commercial software implementation of the FDTD method.

## 2. Influence of the material

The response of a medium to an electric field of pulsation $\omega$ is determined by its dielectric function $\varepsilon(\omega)$. To illustrate the link between $\varepsilon(\omega)$ and the resonant behaviour of nanoparticles (NPs), one can consider a spherical particle with a radius $a$ very small compared to the wavelength of the applied field: $\lambda \gg a$. In this case, the field can be approximated as uniform within the particle dimensions. In this quasistatic approximation, the NP acts as a dipole placed at its centre. The NP dipole moment, $\mathbf{p}$, is linked to the exciting field, $\mathbf{E}_0$, by the relationship $\mathbf{p} = \varepsilon_0\varepsilon_\mathrm{d}\alpha\mathbf{E}_0$, where $\varepsilon_0$ is the vacuum permittivity and $\varepsilon_\mathrm{d}$ is the relative dielectric constant of the embedding medium. Finally, $\alpha$ stands for the NP polarisability, which has the form

$$\alpha = 4\pi a^3 \frac{\varepsilon(\omega) - \varepsilon_\mathrm{d}}{\varepsilon(\omega) + 2\varepsilon_\mathrm{d}}. \quad (1)$$

Equation (1) shows that the polarisability experiences a resonant enhancement when $|\varepsilon(\omega) + 2\varepsilon_\mathrm{d}|$ is minimum, which for small values of $\varepsilon''(\omega) = \mathrm{Im}[\varepsilon(\omega)]$ (low absorption losses), yields

$$\varepsilon'(\omega) = \mathrm{Re}[\varepsilon(\omega)] = -2\varepsilon_\mathrm{d}. \quad (2)$$

This relationship, known as the Fröhlich condition, defines the dipolar LSPR of the spherical NP. This condition can only be fulfilled when the real part of $\varepsilon(\omega)$ is negative, which is the case for metals. We further note that Equation (2) expresses the dependence of the plasmon resonant frequency on the dielectric properties of the surrounding medium, which makes plasmonic NPs ideal for optical sensing. In this article, we focus on optical antennas whose response is governed by dipolar LSPRs. This enables us to neglect the emergence of higher order multipolar resonances in these nanostructures [19,27–29].

In noble metals, the conduction electrons can be considered as non-interacting and free to move within the ionic lattice constituted of the metal nuclei and the tightly bound inner electrons. Using this assumption and introducing an effective damping rate, $\gamma$, it is possible to describe the forces acting on an electron and derive the dielectric function within the so-called Drude model [30]. In this context, we have

$$\varepsilon(\omega) = 1 - \frac{\omega_\mathrm{p}^2}{\omega^2 + \mathrm{i}\gamma\omega}, \quad (3)$$

where $\omega_\mathrm{p}^2 = ne^2/m\varepsilon_0$ is the *plasma frequency* of the metal considered, a constant depending only on material properties: $n$ is the free electron density, $e$ and $m$ its charge and effective mass, and $\gamma$ the aforementioned damping rate. From Equation (3), one can infer that a plasmonic behaviour is possible only for frequencies where $\omega < \omega_\mathrm{p}$ (for small gamma). Metals with $\omega_\mathrm{p}$ in the UV range can sustain surface plasmons in the visible and near-IR range. In this article, we focus on the four main metals fulfilling this condition: silver, gold, copper and aluminium. Note however that metals present significant losses in the visible and ultra-violet (UV) range because of interband electronic transitions [31]. This leads to a deviation from the Drude model mostly expressed by larger imaginary parts of the dielectric function in these wavelength ranges. These interband transitions are usually described through the addition of Lorentz-like terms peaking at high frequencies to Equation (3) [32].

Figure 1 presents the real and imaginary parts of the permittivity for silver, gold, copper and aluminium obtained from [33]. On the one hand, the real part $\varepsilon'(\omega)$ describes the strength of the polarisation induced by the external field. On the other hand, the imaginary part $\varepsilon''(\omega)$ describes the losses. Silver presents the lowest loss across the visible range (400–700 nm), however it is well known that degradation problems generally make it less suitable for plasmonics applications. In contrast, gold is chemically very stable but shows higher losses below 550 nm associated with the occurrence of electronic interband transitions. The dielectric properties of copper are comparable with gold between 600 and 750 nm. If we consider its lower cost, copper could be a good alternative material but unfortunately it is usually not a good choice, mainly because of the fabrication problems associated with its oxidation [34,35]. Finally, aluminium presents large losses around 800 nm associated to interband transitions at this wavelength, therefore it is not an ideal material for optical antennas in the visible regime. However in the UV, away from the absorption band, aluminium is a very promising plasmonic material [36]. Importantly, noble metals are not the only option: West *et al*. [34] have reported a very detailed analysis of the advantages and disadvantages of using alternative plasmonic materials such as semiconductors or metallic alloys. Finally, a recent report has shown that it is possible to maintain the plasmonic properties of silver by passivating the surface of nanostructures with a monolayer of graphene, avoiding the degradation induced by air sulfidation [37].

We discuss the properties of optical nanoantennas based on numerical simulations performed by the FDTD method, using the commercial 3D full-wave electromagnetic wave solver Lumerical FDTD Solutions. The nanostructures are illuminated by a plane wave at an incidence normal to the substrate, with a polarisation along the long axis of the antenna. The material properties of the metals are modelled through the Drude–Lorentz fitting of the dielectric properties shown in Figure 1. We first discuss three key properties of the devices: their scattering and absorption cross-section, and the near-field enhancement they provide. Figure 2(*a*) presents the scattering cross-section of a

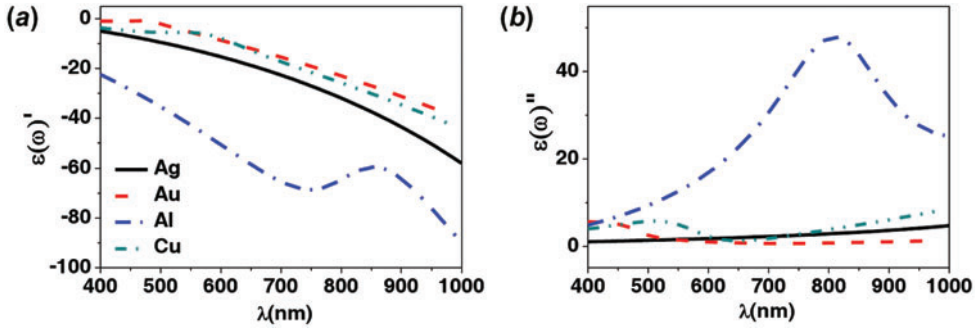


Figure 1. ($a$) Real part $\varepsilon'(\omega)$ and ($b$) imaginary part $\varepsilon''(\omega)$ of the permittivity of Ag, Au, Al and Cu obtained from [33].

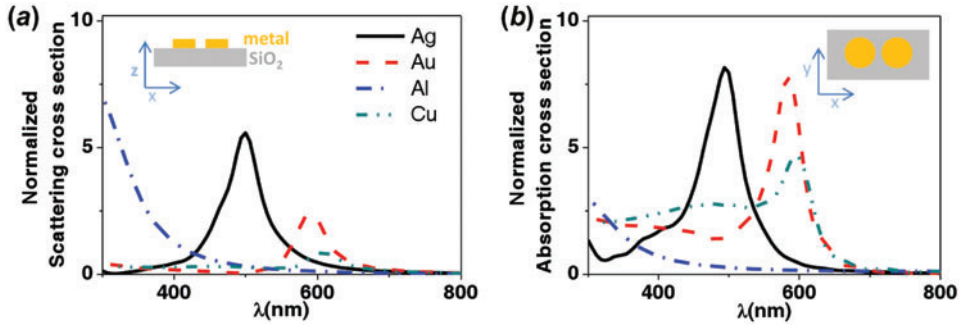


Figure 2. ($a$) Scattering and ($b$) absorption cross-sections of dimer antennas made of Ag, Au, Al and Cu. Insets: Sketch of the nanoantennas composed of two opposing disks with 50 nm diameter and 20 nm thickness separated by a 20 nm gap. For comparison, the cross-sections are normalised to the physical area of the dimer. The antennas are placed on top of a semi-infinite $SiO_2$ substrate with refractive index $n = 1.45$.

nanostructure consisting of two 20 nm-thick opposing disks of 50 nm diameter separated by a 20 nm gap. The cross-sections are normalised to the physical area of the dimer. At resonance, the scattering cross-section is almost one order of magnitude larger than the physical cross-section of the structure. In addition, for the same dimensions, the position of the resonance depends on the material. Al produces strong resonances in the UV, and in the visible range Ag usually allows for the strongest response, at shorter wavelengths than Au and Cu. Figure 2($b$) presents the absorption cross-section of the same structures. This is determined by the imaginary part of the NP polarisability (see Equation (1)), which gives the energy dissipated in the form of work performed by the incident fields on the NP dipole moment. The trends for the position and intensity of the resonance are similar to the ones for the scattering cross-section. Silver presents low loss across the visible range, whereas Au and Cu have interband transitions in the lower wavelength range. This leads to the plateau in absorption below 550 nm for those two materials. Apart from its high losses, Al presents the largest $\varepsilon'(\omega)$ within the visible range, which prevents the incident fields from penetrating into the metal NP, and is thus not usually used for applications in this window.

The ability of nanoantennas to generate high localised fields is another crucial aspect to take into account in the design of suitable devices. Figure 3 continues the material

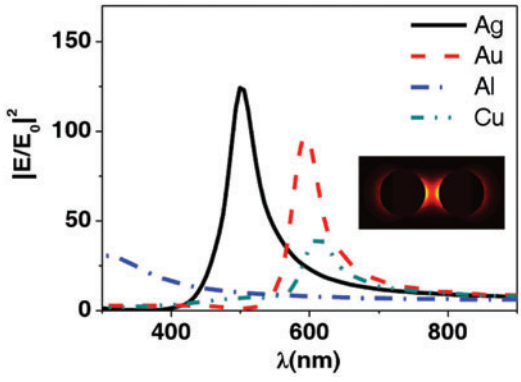


Figure 3. Simulated near-field enhancement at the gap centre, 4 nm above the substrate, of dimer antennas made of Ag, Au, Al and Cu. The antennas' dimensions are identical to those used in Figure 2.

comparison by showing the near-field enhancement at the gap of the dimer antennas. The electromagnetic field is predominately localised in this region when the incident light is polarised along the antenna long axis. The near-field calculations show a tendency similar to the scattering cross-sections, although the wavelength of maximum field intensity is slightly red-shifted compared to the far-field resonances. This effect will be discussed in the following sections. For the rest of the article, gold is taken as the ref-

erence material used in the simulations of the nanoantennas without loss of generality in the physical discussions.

One last material parameter that can influence the properties of nanoantennas is the microstructure of the metal. It has been less studied in the literature than the other parameters, but in the case of gold, for instance, there are evidences that plasmonic structures made out of a highly crystalline metal perform better [38]. This has been tested by making nanoantennas from monocrystalline gold flakes. Moreover, other structures have shown to present a higher scattering cross-section when produced using an adhesion layer allowing for the growth of smoother, highly crystalline gold [39].

## 3. Influence of the dimensions and geometry on the plasmonic properties

The material properties are not the only factor governing the optical response of a nanoantenna: shape and geometry also play a crucial role. In particular, the dimension of the particles parallel to the incident electric field is one of the most determinant factors to control the resonant frequency, the near-field enhancement or the scattering characteristics [40–42]. Indeed, if we consider a single metal nanoparticle as a Fabry–Pérot cavity [5], its resonances will be given by its length; $L = (m/2)\lambda_{\text{eff}}$ where $m$ is an integer number and $\lambda_{\text{eff}}$ the effective wavelength of the plasmon mode [43]. The lowest (dipole) LSPR supported by the metal NP ($m = 1$) is the most intense and the one that determines the resonant wavelength for a dimer antenna composed by two identical NPs.

In order to understand intuitively the dependence of the resonant frequency with the particle length, we can set an analogy between the plasmon mode and an harmonic oscillator. The restoring force in the LSPR originates from the Coulomb interaction between the positive and negative charges induced in the NP. Thus, the larger the distance between the charges (the longer the NP), the smaller the effective spring constant, and the lower the resonant frequency [6]. In dimers, created by placing the two metallic NPs at a distance short enough so that their near fields can interact, the dimension of the gap between the two arms of the antenna also affects its plasmonic resonances [44]. In this case, a red-shift of the dimer LSPR is induced, compared with the single particle case. The hybridisation model [44,45] explains this red-shift as a result of the electrostatic mixture of different energy levels associated with different charge distributions at the isolated NPs [46,47]. According to this intuitive picture, the configuration that minimises the distance between charges of opposite sign corresponds to the lowest energy dimer resonance. Figure 4 shows the normalised scattering cross-section (*a*) and the near-field intensity (*b*) for 100 nm long, 40 nm wide and 45 nm thick NPs separated by gap distances between 5 and 40 nm. When the gap size is reduced, the scattering resonance and the near-field maxima (evaluated at the centre of the gap) shift to lower energies (longer wavelengths). Note that, due to the evanescent nature of the plasmonic fields, the near-field intensity increases exponentially with reducing gap size. This fact illustrates the importance of obtaining small gaps, which is one of the main fabrication challenges in the production of efficient nanoantennas [48].

Figure 5(*a*) illustrates the importance of the length of each of the NPs in a dimer antenna, it shows the evolution of the spectral position of the far-field scattering maximum (*a*) and near-field intensity enhancement (*b*) for the case of dimer antennas with different arm lengths (for a fixed 20 nm gap distance). Note that the near-field intensity is evaluated at the antenna gap. It is noticeable that modifying the antenna arm length by just 40 nm allows for a wide tunability range of approximately 200 nm. The spatial distribution of the near-field enhancement shows a significant increase of the intensity at the gap as the antenna arm length increases (Figure 5(*b*)). This can be understood as the result of an effective increase of the coupling strength between the two antenna arms. As the antenna arm increases, the gap has a smaller size relative to the resonant wavelength, which results in a stronger coupling between the LSPRs supported by both arms. Experimentally, the field distribution around a nanoantenna – i.e. the information presented in Figure 5(*b*) – can be measured using a technique called scanning near field optical microscopy, which allows for the mapping of optical fields on scales smaller than the diffraction limit. This method has been used to confirm the field distribution around nanoantennas such as the ones discussed in the present article [49–51]. For further information on experimental methods allowing for the spatial mapping of nanoscale optical fields, we refer the reader to the review articles [29,52].

An effect often overlooked is that the maximum near-field intensity in the surroundings of the antenna occurs at a wavelength different from that of maximum scattering [21,23,24,53]. In the following, we will refer to this as the shift between near-field and far-field, $\Delta\lambda = \lambda_{\text{nf}}^{\text{peak}} - \lambda_{\text{ff}}^{\text{peak}}$. This can be explained directly by the physics of a driven and damped harmonic oscillator. Zuloaga *et al.* [23] showed that this shift depends directly on the total damping of the system; intrinsic damping within the metal of the nanoparticle and radiative damping of the localised plasmon. However, in the close vicinity of the nanostructure, $\Delta\lambda$ depends on the position. This is shown in the right hand side column of Figure 5(*b*) which presents the spatial distribution of $\Delta\lambda$ for antennas with arm length of 100, 140 and 180 nm. In the zones where the enhancement is maximal, i.e. in the gap and at the extremities of each arm of the dimer, a significant red shift is observed in all three cases. Figure 5(*a*) shows that the shift in the gap increases with the antenna arm length, up to a value of 30 nm for the 180 nm case in the near-infrared spectral regime. If we consider that optical antennas are generally characterised by

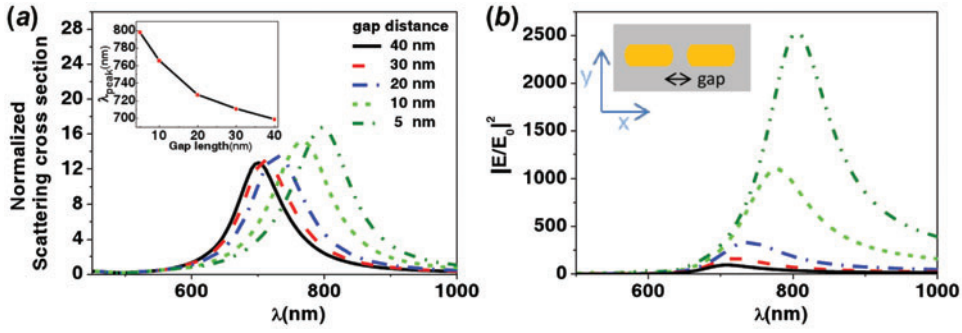


Figure 4. (*a*) Evolution of the scattering cross-section with the antenna gap. Inset: dependence of the scattering peak wavelength with the gap distance. The cross-sections are normalised to the physical area of the dimer. (*b*) Near-field intensity enhancement at the gap centre ($z = 22$ nm) as a function of the incident frequency for different gap sizes. The particle length (100 nm), width (40 nm) and the thickness (45 nm) are fixed in all cases. The antennas are sitting on a glass substrate ($n = 1.45$).

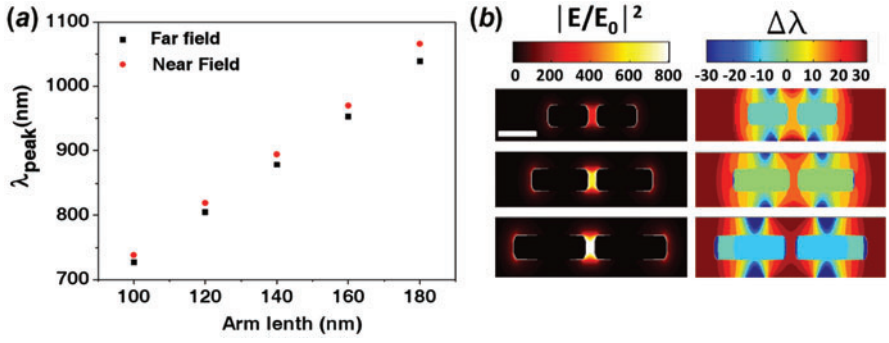


Figure 5. (*a*) Evolution of the wavelength of maximum far-field scattering and near-field intensity for dimer antennas with different arm length. (*b*) Left column: X–Y Spatial distribution of the near-field enhancement around the antenna at the middle height of the particles ($z = 22$ nm) obtained at resonance for different antenna arm lengths (scale bar: 100 nm). Right column: spatial distribution of the wavelength resonance shift, $\Delta\lambda = \lambda_{nf}^{peak} - \lambda_{ff}^{peak}$ in nm. The gold nanoantenna gap (20 nm), the particle width (40 nm) and the thickness (45 nm) are fixed in the three cases: 100, 140 and 180 nm arm length. The structures are sitting on a glass substrate ($n = 1.45$).

experimental techniques in the far-field, such as dark-field spectroscopy or Fourier transform infrared spectroscopy (FTIR), the energy shift between far and near-field must be considered in the fabrication process. In particular, applications such as SERS can be very sensitive to this effect as the mechanism influencing their efficiency is the near-field enhancement and not the scattering properties of the antenna [22,54].

Apart from the antenna length and the gap distance, the shape of the particle also affects significantly its LSPRs [55]. Figure 6 highlights the influence of geometry on the antenna properties. For the calculations, we consider NPs with different shapes: bow-ties, rods, ellipsoids, disks and squares. Although the length of the particles parallel to the incident field polarisation and the dimer gap are fixed to 100 nm and 20 nm respectively, the comparison shows a clear effect of the particle width and shape on the energy and strength of the antenna LSPR. Ellipsoids were chosen with the semi-principal axes matching the width and length of the rods to evaluate the effect of sharp edges. The ellipsoidal disks present a blue-shift of 40 nm in the scattering cross-section with respect to the rods (Figure 6(*a*)). Similarly, the disk-dimer resonant wavelength shows a more apparent blue-shift, 70 nm, compared to the square dimer. There are two reasons that cause this blue shift. On the one hand, due to their round shape, the disks present an effective reduction of the particle length along the polarisation direction (<100 nm) compared to the rod or the square. On the other hand, the charge distribution along the curved surface of the disks results in an effective increase of the gap distance (>20 nm) which also contributes to the observed spectral blue-shift. It is particularly important to consider this effect in the design of nanoantennas, when fabrication constraints limit the production of sharp edges.

The scattering and the near-field enhancement comparison in Figure 6 shows a drastic reduction of the strength of the resonances for the geometries with smaller aspect ratio (disks and squares). This effect is caused by the increase of the radiative plasmon damping that occurs in wider NPs [56,57]. In addition, the spatial distribution of the shift between near- and far-field resonances in Figure 6(*b*) shows a larger $\Delta\lambda$ at the gap region for these geometries.

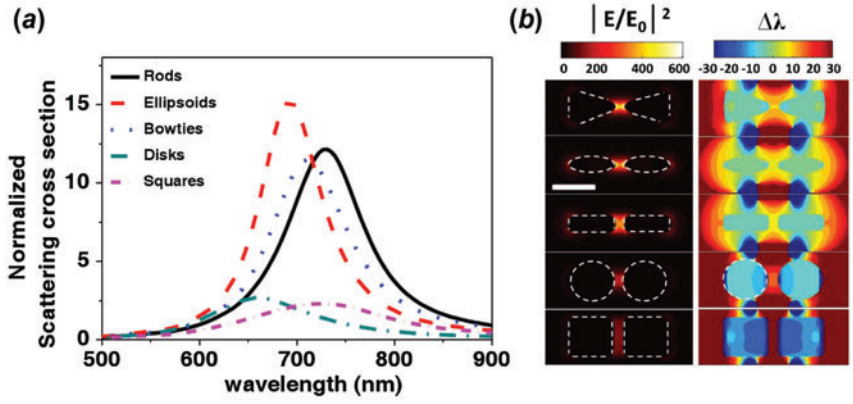


Figure 6. (*a*) Scattering cross-section of antenna dimers with different geometries. (*b*) Left column: field enhancement around the antenna at the resonance wavelength for different dimers: bow-ties, ellipsoids, rods, disks and squares. The cross-sections are normalised to the physical area of the dimer in each case. Right column: spatial distribution of the far-to-near-field resonance shift $\Delta\lambda$ in nm. Scale bar: 100 nm. The arm length in the horizontal direction is 100 nm in all cases. The gold nanoantenna gap and the thickness are set to 20 nm and 45 nm respectively, and the antennas are lying on a glass substrate ($n = 1.45$).

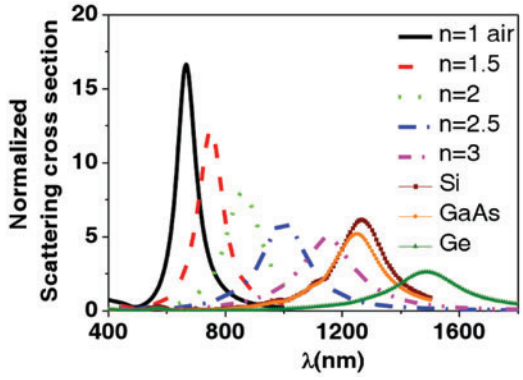


Figure 7. Scattering cross-section spectra of dimer antennas for different substrate refractive indices. Si, GaAs, and Ge substrates were simulated from experimental dielectric data taken from Ref. [62]. The dimer is made of two opposing 100 nm long, 40 nm wide, 45 nm thick rods separated by a 20 nm gap. The cross-sections are normalised to the physical area of the dimer.

Antennas with high aspect ratio, like rod dimers, present intense plasmon resonances that provide high values of near-field enhancement at the gap region. Moreover, such nanoantennas exhibit only a moderate near-to-far-field shift ($\approx$10 nm in the visible range). On the other hand, for applications and devices that require the use of NPs with high aspect ratio such as disks or spheres, it is recommendable to take this shift into account in the design and fabrication processes.

## 4. Influence of substrate on the plasmonic properties

The Fröhlich condition discussed earlier (Equation (2)) illustrates the dependence of the plasmon resonances of spherical NPs on the dielectric properties of the surrounding medium. The resonant wavelength of plasmonic nanoparticles is gradually shifted to longer wavelengths as the surrounding refractive index increases [58]. It has been experimentally demonstrated that the refractive index of the substrate affects the plasmonic properties of the nanoantennas [59–61]. Figure 7 shows the evolution of the scattering cross-section of a gold antenna with the refractive index of the substrate. Apart from a spectral red-shift, increasing the surrounding refractive index enlarges the damping losses experienced by the NPs LSPR. Note that the scattering maxima are broadened and lowered with higher refractive index environment. This is caused by the larger phase difference of the fields in one LSPR oscillation within the substrate medium compared with the vacuum (air) side. Hence, using the substrate with the lowest refractive index possible yields the highest quality factor resonances. The interaction of nanoantennas with semiconducting materials with high refractive index such as Si, Ge or GaAs moves the antenna resonance into the near-infrared. This resonance red-shift must be taken into account in the design of nanoantennas for applications requiring the use of large refractive index substrates. In these configurations, introducing a $SiO_2$ gap of several hundreds of nanometres between the antenna and the substrate can reduce this effect [63].

## 5. Introduction of a reflective layer

Recent studies have demonstrated that the addition of a metal underlay on a glass substrate is a very effective means to increase the field enhancement and the scattering efficiency of metal nanoantennas. This phenomenon, explained by the near-field coupling between the antenna and its mirror image at the metal layer [64], has been used to improve the SERS efficiency [65] and the directivity of antennas [66], allowing for single molecule detection [67]. Moreover, the reflective underlayer provides additional ways of tuning optical antennas by changing the dielectric layer thickness, which can lead to an increasing of near-field enhancement

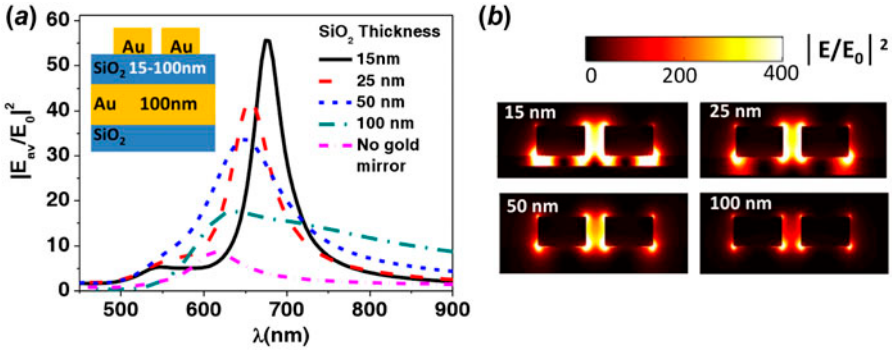


Figure 8. (*a*) Spatially averaged near-field intensity enhancement. The inset shows the sample cross-view. (*b*) Cross-view of the field enhancement distribution, at the peak wavelength of the resonance, for different separations between the nanoantenna and the gold underlayer. The antennas are composed of two opposing 75 nm long, 40 nm wide and 40 nm thick NPs separated by a 30 nm gap.



or quality factors [68]. Figure 8(*a*) shows the spatially averaged near-field enhancement, $E_{\mathrm{av}}/E_0$, as a function of the excitation wavelength. The antennas are composed of two opposing 75 nm long, 40 nm wide and 40 nm thick NPs separated by a 30 nm gap. The field intensity is averaged within a $300\times200\times100\,\mathrm{nm}^3$ volume around the antenna for different $SiO_2$ thicknesses (see inset). This comparison shows enhancement factors up to five times larger than the case without reflective layer, for a 25 nm-thick $SiO_2$ layer. The near-field interaction between the NPs and the gold underlayer causes a significant resonance shift to lower frequencies when the $SiO_2$ layer decreases. This can be explained by the hybridisation of the antenna LSPR with its image in the Au substrate film, which leads to a lowering of the resonance energy when the distance between them is reduced [69]. The cross-views of the near-field intensity distribution corresponding to the different $SiO_2$ separations are shown in Figure 8(*b*). These are evaluated at resonance and illustrate the increase in the near-field enhancement at the gap as the $SiO_2$ separation shrinks. The interaction between the nanostructure LSPR and its image in the reflective layer also improves drastically the radiative properties of the dimer antenna [70].

It is possible to use an optical antenna to modify the absorption and radiative properties of a nanoemitter placed in its vicinity. One of the main effects that the antenna has on the emitter is the modification of its radiative decay rate [7]. The radiative decay rate enhancement experienced by a dye molecule placed next to a nanoantenna is presented in Figure 9 (the antenna dimensions are identical to those in Figure 8). The emitter is modelled through a dipole source with an intrinsic decay rate $\gamma_0$, and it is placed at the centre of the gap, oriented parallel to the main axis of the dimer. In such configuration, the nanoemitter experiences a maximum radiative enhancement ($\gamma_{\mathrm{r}}/\gamma_0 \sim 25$) thanks to its optimal location and orientation with respect to the nanoantenna. When the reflector layer is incorporated, this maximum enhancement increases up to 8 times. A reduction of the $SiO_2$ thickness results in an increase of the maximum

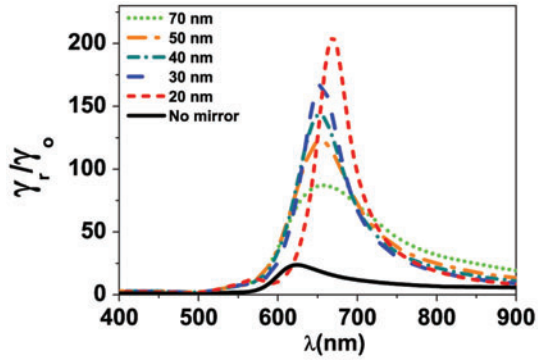


Figure 9. Radiative decay rate enhancement, $\gamma_r/\gamma_0$, for a single emitter placed at the antenna gap and oriented along the antenna axis for different distances between the antenna and the gold underlayer. The antenna geometry is the same as in Figure 8.

value of $\gamma_{\mathrm{r}}/\gamma_0$ as well as in a shift of the wavelength at which the maximum enhancement occurs to longer wavelengths. It is noticeable that the evolution shown in Figure 9, for a single emitter as light source, presents a similar tendency to the predicted results for the maximum near field enhancement of the antenna under plane wave illumination in Figure 8. Note that at very small thickness separations ($t \sim$ 20–30 nm), the enhancement of the non-radiative decay rate outweighs the radiative channel. In that direction, Seok *et al.* [64] demonstrated that the optimum separation is achieved when the radiation quality factor is equal to the absorption quality factor.

## 6. Influence of an adhesion layer

One of the main disadvantages of using gold nanoantennas on glass substrates is their poor adhesion. This is due to the absence of an intermediate oxide layer in the gold evaporation process [71]. Therefore the addition of a few nanometres thick layer of another material between the gold NPs and the substrate surface is generally used for most nanoantenna designs. Despite the thin character of the adhesion layer, it influences the performance of the nanoantenna: the LSPR

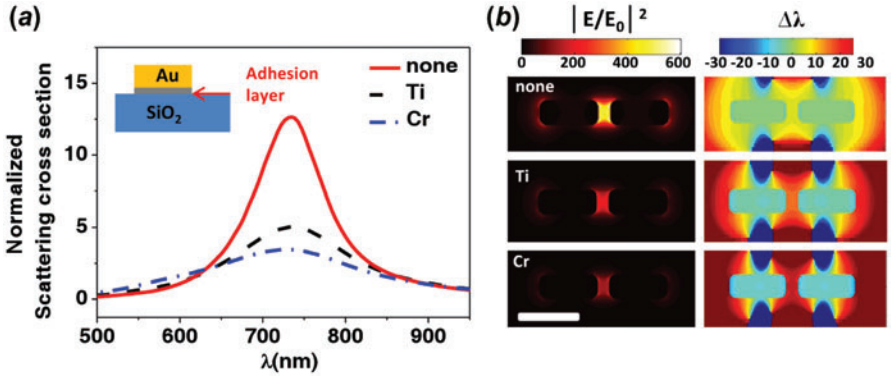


Figure 10. (*a*) Scattering cross-section spectra of a gold antenna dimer for different adhesion layers. (*b*) Left column: spatial field enhancement distribution around the antenna at resonance (Scale bar: 100 nm). Right column: spatial distribution of the near-to-far-field shift $\Delta\lambda$ in nm. The dielectric functions of Ti, Cr, and $SiO_2$ are taken from Ref. [62]. The thickness of the adhesion layer is set to 4 nm. The antennas consist of two opposing rods 100 nm long, 40 nm wide and 45 nm thick, separated by a 20 nm gap. The cross-sections are normalised to the physical area of the dimer.

is highly sensitive to the environment. The presence of the adhesion layer leads to a red-shift of the plasmon resonance and to a significant increase of its spectral width [72]. It has been demonstrated experimentally that the presence of such a layer significantly deteriorates the properties of plasmonic devices [73–76]. $TiO_2$ is considered as the best material to use as an adherent in terms of reducing the deterioration of the plasmonic properties of nanoantennas [73,77].

The effect of ultrathin adhesion layers of Cr and Ti on the LSPR supported by a gold dimer on a gold substrate is shown in Figure 10. The scattering intensity drops drastically, with a reduction of 55% for Ti and 65% for Cr (see panel (*a*)). The same reduction is observed in the near-field enhancement at the gap, see Figure 10(*b*). Note that the additional damping channel introduced by the adhesion layer causes a further energy shift between near and far-field resonances (30 nm for Cr). This effect must be considered alongside with the other sources of near-to-far field spectral shift discussed in Figures 5(*a*) and (*b*). An elegant solution around this problem, when gold is concerned, is the use of a molecular linker which acts as a sticking layer and does not introduce any additional damping. It has been reported that such strategy maintains, if not improves, the plasmonic properties of optical antennas [39].

## 7. Antennas arrays and near-field enhancement

The near-field enhancement can be further increased by arranging the nanoantennas in periodic arrays. The coupling between grating modes and the LSPRs in NP arrays leads to narrow resonances in the near and far field that can be particularly suitable for sensing applications [78–80]. Such coupling has previously been demonstrated in the optical regime, and it can also be scaled to the THz range with the purpose of detecting changes in the refractive indices of fluids placed on the antenna array [81]. Calculations predict that gold NP arrays can exhibit near-field enhancements

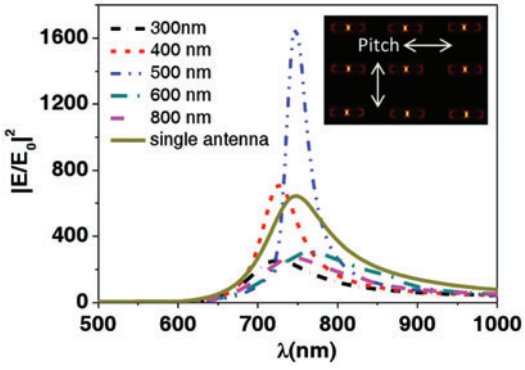


Figure 11. Near-field enhancement at the gap of periodic arrays of antenna dimers for different pitches. The inset shows the sample plane view, and illustrates the field enhancement localised at the gap of the antennas at resonance. Each nanoantenna is composed of two opposing 100 nm long, 40 nm wide, 40 nm thick arms separated by a 20 nm gap. The antennas are placed on a glass substrate of index $n = 1.45$.

approximately one order of magnitude greater than those of isolated NPs [82–84]. Figure 11 shows the near-field enhancement at the gap for square arrays of dimer antennas with different periods, $d$. A narrow near-field resonance is observed for $d = 500$ nm. The optimum periodic distance occurs at the first grating order, and it can be easily estimated from the resonance of a single nanoantenna $\lambda_{res}$ and the refractive index of the antenna substrate $n$, $d = \lambda_{res}/n$ [82].

## 8. Conclusions

We have reviewed numerically the factors that generally control the performances of optical antennas. These include intrinsic aspects such as the dielectric properties of the metal used or the geometry of the antenna, and extrinsic factors such as the substrate or the presence of reflective or adhesion layers. We have shown that the maximum in

the near field intensity occurs at a wavelength different from that of maximum scattering cross-section. We have emphasised that the near- to far-field shift on dimer antennas is highly influenced by many parameters. An optimum configuration providing high near-field enhancement and scattering efficiency would consist of nanoantenna dimers composed by NPs with high aspect ratio, arranged in a periodic fashion on top of a low-refractive-index substrate without the need of an adhesion layer. The inclusion of a gold metal underlayer would even improve the quality factor of the LSPR supported by such a system. All these practical factors should be considered when designing plasmonic nanoantenna devices for specific applications.

## Funding

This work is funded by the UK Engineering and Physical Sciences Research Council (EPSRC), the Leverhulme Trust and Nano-Sci Era Nanospec.

## Note

1. www.lumerical.com

## Notes on contributors

Roberto Fernández-García studied physics at the University of Oviedo (Spain). He obtained his M.S. and Ph.D. degree in material physics in 2009 and 2010 at the Universidad Autónoma de Madrid (Spain), in collaboration with the Instituto de Ciencia de Materiales de Madrid (ICMM) in 2010. In 2009 he joined Imperial College London as a Ph.D. student, where he moved into the study of optical nanoantennas using microscopy, spectroscopy and numerical calculations.

Yannick Sonnefraud obtained his PhD at the Université Joseph Fourier, Grenoble (France) in 2007, focusing on Near-field Scanning Optical Microscopy. He then joined Imperial College London as a postdoctoral research associate, where his interests are in the study of plasmonics systems using optical imaging and spectroscopic methods. He has been awarded a Leverhulme Fellowship in 2010, and appointed as researcher at the Institut Néel in Grenoble in 2013. His research interests are still linked to plasmonics, with an emphasis on nanoantennas and plasmonics in the quantum regime.

Antonio I. Fernández-Domínguez received M.S. and Ph.D. (Hons) degrees in condensed matter physics from the Universidad Autónoma de Madrid, Spain, in 2004 and 2009, respectively. Since then, he has been working in the field of theoretical plasmonics and metamaterials as a Marie Curie fellow in the Department of Physics, Imperial College London, UK.

Vincenzo Giannini studied physics at the University of Pisa (Italy). He achieved his Ph.D. in theoretical condensed matter physics at Universidad Autónoma de Madrid (Spain) working on the strong interaction of light with metal nanoparticles and the excitation of localised surface plasmons. He then had a joint postdoctoral position at the FOM Institute for Atomic and Molecular Physics (AMOLF) in Amsterdam and at Philips Research in Eindhoven. He is currently a research fellow in the Physics Department at Imperial College London where his research interests include theoretical plasmonics and nano-optics.

Stefan A. Maier is Professor of Nanophotonics in the Physics Department and a Co-Director of the Centre for Plasmonics & Metamaterials at Imperial College London. In 2009, he also became Visiting Professor at A*STAR Institute for Materials Research & Engineering (IMRE), Singapore. Research in his group comprises fundamental light/matter interactions on the nanoscale as well as applied design of metamaterials, now aspiring to integrated biological sensors. Stefan is a Fellow of the Optical Society of America. His contributions to nanostructured optical metallic waveguides and high-confinement plasmon waveguiding in the terahertz regime found much acclaim in the surging field of plasmonics, earning him the Paterson medal and the Sackler Prize in Physics in 2010.

## References

[1] K.B. Crozier, A. Sundaramurthy, G.S. Kino, and C.F. Quate, *Optical antennas: Resonators for local field enhancement*, J. Appl. Phys. 94 (2003), p. 4632.
[2] P.J. Schuck, D.P. Fromm, A. Sundaramurthy, G.S. Kino, and W.E. Moerner, *Improving the mismatch between light and nanoscale objects with gold bowtie nanoantennas*, Phys. Rev. Lett. 94 (2005), pp. 14–17.
[3] J.A. Schuller, T. Taubner, and M.L. Brongersma, *Optical antenna thermal emitters*, Nat. Photonics 3 (2009), pp. 658–661.
[4] Q.H. Park, *Optical antennas and plasmonics*, Contemp. Phys. 50 (2009), pp. 407–423.
[5] V. Giannini, A.I. Fernández-Domínguez, S.C. Heck, and S.A. Maier, *Plasmonic nanoantennas: fundamentals and their use in controlling the radiative properties of nanoemitters*, Chem. Rev. 111 (2011), pp. 3888–912.
[6] P. Biagioni, J. Huang, and B. Hecht, *Nanoantennas for visible and infrared radiation*, Rep. Prog. Phys. 75 (2012), p. 024402.
[7] V. Giannini, A.I. Fernández-Domínguez, Y. Sonnefraud, T. Roschuk, R. Fernández-García, and S.A. Maier, *Controlling light localization and light-matter interactions with nanoplasmonics*, Small 6 (2010), pp. 2498–507.
[8] P. Bharadwaj, B. Deutsch, and L. Novotny, *Optical Antennas*, Adv. Opt. Photonics 1 (2009), p. 438.
[9] L. Novotny, and N. Hulstvan, *Antennas for light*, Nat. Photonics 5 (2011), pp. 83–90.
[10] J.A. Schuller, E.S. Barnard, W. Cai, Y.C. Jun, J.S. White, and M.L. Brongersma, *Plasmonics for extreme light concentration and manipulation*, Nat. Mater. 9 (2010), pp. 193–204.

[11] M.I. Stockman, *Nanoplasmonics: past, present, and glimpse into future*, Opt. Express 19 (2011), p. 22029.

[12] S. Nie, *Probing single molecules and single nanoparticles by surface-enhanced Raman scattering*, Science 275 (1997), pp. 1102–1106.

[13] K. Kneipp, Y. Wang, H. Kneipp, L. Perelman, I. Itzkan, R. Dasari, and M. Feld, *Single molecule detection using surface-enhanced Raman scattering (SERS)*, Phys. Rev. Lett. 78 (1997), pp. 1667–1670.

[14] G. Volpe, M. Noack, S.S. Aćimović, C. Reinhardt, and R. Quidant, *Near-field mapping of plasmonic antennas by multiphoton absorption in poly(methyl methacrylate)*, Nano Lett. 12 (2012), pp. 4864–4868.

[15] E. Boisselier, and D. Astruc, *Gold nanoparticles in nanomedicine: preparations, imaging, diagnostics, therapies and toxicity*, Chem. Soc. Rev. 38 (2009), pp. 1759–1782.

[16] D. Lapotko, *Plasmonic nanoparticle-generated photothermal bubbles and their biomedical applications*, Nanomed. London England 4 (2009), pp. 813–845.

[17] X. Liu, M.C. Lloyd, I.V. Fedorenko, P. Bapat, T. Zhukov, and Q. Huo, *Enhanced imaging and accelerated photothermalysis of A549 human lung cancer cells by gold nanospheres*, Nanomed. London England 3 (2008), pp. 617–626.

[18] H.A. Atwater, and A. Polman, *Plasmonics for improved photovoltaic devices*, Nat. Mater. 9 (2010), p. 865.

[19] M. Stewart, C. Anderton, L. Thompson, J. Maria, S.K. Gray, J.A. Rogers, and R. Nuzzo, *Nanostructured plasmonic sensors*, Chem. Rev. 108 (2008), p. 494.

[20] S. Linic, P. Christopher, and D.B. Ingram, *Plasmonic-metal nanostructures for efficient conversion of solar to chemical energy*, Nat. Mater. 10 (2011), pp. 911–921.

[21] F. Moreno, P. Albella and M. Nieto-Vesperinas, *Analysis of the spectral behavior of localized plasmon resonances in the near- and far-field regimes*, Langmuir 29 (2013), pp. 6715–6721.

[22] B.M. Ross and L.P. Lee, *Comparison of near- and far-field measures for plasmon resonance of metallic nanoparticles*, Opt. Lett. 34 (2009), pp. 896–898.

[23] J. Zuloaga and P. Nordlander, *On the energy shift between near-field and far-field peak intensities in localized plasmon systems*, Nano Lett. 11 (2011), pp. 1280–1283.

[24] P. Alonso-González, P. Albella, F. Neubrech, C. Huck, J. Chen, F. Golmar, F. Casanova, L.E. Hueso, A. Pucci, J. Aizpurua, and R. Hillenbrand, *Experimental verification of the spectral shift between near- and far-field peak intensities of plasmonic infrared nanoantennas*, Phys. Rev. Lett. 110 (2013), pp. 203902.

[25] A. Taflove and S. Hagness, *Artech House Antennas and Propagation Library*, Artech House, London, 2000.

[26] K. Yee, *Numerical solution of initial boundary value problems involving maxwell's equations in isotropic media*, IEEE Trans. Antennas Propag. 14 (1966), pp. 302–307.

[27] T. Chung, S.Y. Lee, E.Y. Song, H. Chun and B. Lee, *Lee, Plasmonic nanostructures for nano-scale bio-sensing,* sensors 11 (2011), pp. 10907–10929.

[28] D.Y. Lei, K. Appavoo, Y. Sonnefraud, J. Richard, F. Haglund, and S.A. Maier, *Single-particle plasmon resonance spectroscopy of phase transition in vanadium dioxide*, Opt. Lett. 35 (2010), pp. 3988–3990.

[29] Y. Sonnefraud, A. Leen Koh, D. McComb, and S. Maier, *Nanoplasmonics: Engineering and observation of localized plasmon modes*, Laser Photonics Rev. 6 (2012), p. 277.

[30] S.A. Maier, *Plasmonics - Fundamentals and applications*, Physics 76 (2010), p. 223.

[31] P.B. Johnson and R.W. Christy, *Optical Constants of the Noble Metals*, Phys. Rev. B 6 (1972), pp. 4370–4379.

[32] S.G. Rodrigo, F.J. García-Vidal and L. Martín-Moreno, *Influence of material properties on extraordinary optical transmission through hole arrays*, Phys. Rev. B 77 (2008), p. 075401.

[33] D.R. Lide, editor, *CRC Handbook of Chemistry and Physics*, 84th ed., CRC Press, Boca Raton, FL, 2003, pp. 504–504.

[34] P. West, S. Ishii, G. Naik, N. Emani, V.M. Shalaev, and A. Boltasseva, *Searching for Better Plasmonic Materials*, Laser Photonics Rev. 4 (2009), p. 27.

[35] G.H. Chan, J. Zhao, E.M. Hicks, G.C. Schatz and R.P. Van Duyne, *Plasmonic properties of copper nanoparticles fabricated by nanosphere lithography*, Nano Lett. 7 (2007) pp. 1947–1952.

[36] L. Li, S.F. Lim, A.A. Puretzky, R. Riehn and H.D. Hallen, *Near-field enhanced ultraviolet resonance Raman spectroscopy using aluminum bow-tie nano-antenna*, Appl. Phys. Lett. 101 (2012), p. 113116.

[37] J.C. Reed, H. Zhu, A.Y. Zhu, C. Li, and E. Cubukcu, *Graphene-enabled silver nanoantenna sensors*, Nano Lett. 12 (2012), pp. 4090–4094.

[38] J.S. Huang, V. Callegari, P. Geisler, C. Brüning, J. Kern, J.C. Prangsma, X. Wu, T. Feichtner, J. Ziegler, P. Weinmann, M. Kamp, A. Forchel, P. Biagioni, U. Sennhauser, and B. Hecht, *Atomically flat single-crystalline gold nanostructures for plasmonic nanocircuitry*, Nat. Commun. 1 (2010), p. 150.

[39] T.G. Habteyes, S. Dhuey, E. Wood, D. Gargas, S. Cabrini, P.J. Schuck, A.P. Alivisatos, and S.R. Leone, *Metallic adhesion layer induced plasmon damping and molecular linker as a nondamping alternative*, ACS Nano 6 (2012), pp. 5702–5709.

[40] H. Kuwata, H. Tamaru, K. Esumi, and K. Miyano, *Resonant light scattering from metal nanoparticles: Practical analysis beyond Rayleigh approximation*, Appl. Phys. Lett. 83 (2003), p. 4625.

[41] B.J. Wiley, Y. Chen, J.M. McLellan, Y. Xiong, Z.Y. Li, D. Ginger, and Y. Xia, *Synthesis and optical properties of silver nanobars and nanorice*, Nano Lett. 7 (2007), pp. 1032–1036.

[42] Z. Liu, A. Boltasseva, R. Pedersen, R. Bakker, A. Kildishev, V. Drachev, and V. Shalaev, *Plasmonic nanoantenna arrays for the visible*, Metamaterials 2 (2008), pp. 45–51.

[43] E. Massa, S.A. Maier, and V. Giannini, *An analytical approach to light scattering from small cubic and rectangular cuboidal nanoantennas*, New J. Phys. 15 (2013), p. 063013.

[44] H. Fischer, and O.J.F. Martin, *Engineering the optical response of plasmonic nanoantennas*, Opt. Express 16 (2008), pp. 9144–9154.

[45] E. Prodan, C. Radloff, N.J. Halas, and P. Nordlander, *A hybridization model for the plasmon response of complex nanostructures*, Science 302 (2003), pp. 419–422.

[46] A. Aubry, D.Y. Lei, S.A. Maier, and J.B. Pendry, *Interaction between plasmonic nanoparticles revisited with transformation optics*, Phys. Rev. Lett. 105 (2010), p. 233901.

[47] J.B. Pendry, A.I. Fernández-Domínguez, Y. Luo, and R. Zhao, *Capturing photons with transformation optics*, Nat. Phys. 9 (2013), pp. 518–522.

[48] H. Duan, A.I. Fernández-Domínguez, M. Bosman, S.A. Maier, and J.K.W. Yang, *Nanoplasmonics: Classical down to the nanometer scale*, Nano Lett. 12 (2012), pp. 1683–1689.

[49] R.L. Olmon, P.M. Krenz, A.C. Jones, G.D. Boreman, and M.B. Raschke, *Near-field imaging of optical antenna modes in the mid-infrared*, Opt. Express 16 (2008), pp. 20295–20305.

[50] M. Schnell, A. García-Etxarri, A.J. Huber, K. Crozier, J. Aizpurua, and R. Hillenbrand, *Controlling the near-field oscillations of loaded plasmonic nanoantennas*, Nat. Photonics 3 (2009), p. 287.

[51] J. Dorfmüller, R. Vogelgesang, W. Khunsin, C. Rockstuhl, C. Etrich, and K. Kern, *Plasmonic nanowire antennas: Experiment, simulation, and theory*, Nano Lett. 10 (2010), pp. 3596–3603.

[52] R. Vogelgesang, and A. Dmitriev, *Real-space imaging of nanoplasmonic resonances*, Analyst 135 (2010), pp. 1175–1181.

[53] B.M. Ross, and L.P. Lee, *Comparison of near- and far-field measures for plasmon resonance of metallic nanoparticles*, Opt. Lett. 34 (2009), pp. 896–8.

[54] M.D. Doherty, A. Murphy, R.J. Pollard, and P. Dawson, *Surface-enhanced Raman scattering from metallic nanostructures: Bridging the gap between the near-field and far-field responses*, Phys. Rev. X 3 (2013), p. 011001.

[55] J.J. Mock, M. Barbic, D.R. Smith, D.A. Schultz, and S. Schultz, *Shape effects in plasmon resonance of individual colloidal silver nanoparticles*, J. Phys. Chem. 116 (2002), p. 6755.

[56] K.S. Lee, and M.A. El-Sayed, *Gold and silver nanoparticles in sensing and imaging: sensitivity of plasmon response to size, shape, and metal composition*, J. Phys. Chem. B 110 (2006), pp. 19220–19225.

[57] J. Becker, A. Trügler, A. Jakab, U. Hohenester, and C. Sönnichsen, *The optimal aspect ratio of gold nanorods for plasmonic bio-sensing*, Plasmonics 5 (2010), pp. 161–167.

[58] J.J. Mock, D.R. Smith, and S. Schultz, *Local refractive index dependence of plasmon resonance spectra from individual nanoparticles*, Nano Lett. 3 (2003), pp. 485–491.

[59] A. Curry, G. Nusz, A. Chilkoti, and A. Wax, *Substrate effect on refractive index dependence of plasmon resonance for individual silver nanoparticles observed using darkfield micro-spectroscopy*, Opt. Express 13 (2005), pp. 2668–2677.

[60] M. Valamanesh, Y. Borensztein, C. Langlois, and E. Lacaze, *Substrate effect on the plasmon resonance of supported flat silver nanoparticles*, J. Phys. Chem. C 115 (2011), pp. 2914–2922.

[61] B. Auguié, X.M. Bendaña, W.L. Barnes, and F.J. Garcìa de Abajo, *Diffractive arrays of gold nanoparticles near an interface: Critical role of the substrate*, Phys. Rev. B 82 (2010), p. 155447.

[62] E.D. Palik, Academic Press, New York 1 (1985), p. 804.

[63] S. Heeg, R. Fernández-García, A. Oikonomou, F. Schedin, R. Narula, S.A. Maier, A. Vijayaraghavan, and S. Reich, *Polarized plasmonic enhancement by Au nanostructures probed through Raman scattering of suspended graphene*, Nano Lett. 13 (2013), pp. 301–308.

[64] T.J. Seok, A. Jamshidi, M. Kim, S. Dhuey, A. Lakhani, H. Choo, P.J. Schuck, S. Cabrini, A.M. Schwartzberg, J. Bokor, E. Yablonovitch, and M.C. Wu, *Radiation engineering of optical antennas for maximum field enhancement*, Nano Lett. 11 (2011), pp. 2606–10.

[65] Y. Chu, D. Wang, W. Zhu, and K.B. Crozier, *Double resonance surface enhanced Raman scattering substrates: an intuitive coupled oscillator model*, Opt. Express 19 (2011), pp. 14919–28.

[66] D. Wang, W. Zhu, Y. Chu, and K.B. Crozier, *High directivity optical antenna substrates for surface enhanced Raman scattering*, Adv. Mater. (Deerfield Beach, FL) 24 (2012), pp. 4376–80.

[67] A. Ahmed, and R. Gordon, *Single molecule directivity enhanced Raman scattering using nanoantennas*, Nano Lett. 12 (2012), pp. 2625–30.

[68] D. Gramotnev, A. Pors, M. Willatzen, and S. Bozhevolnyi, *Gap-plasmon nanoantennas and bowtie resonators*, Phys. Rev. B 85 (2012), p. 045434.

[69] E. Prodan, C. Radloff, N. Halas, and P. Nordlander, *A hybridization model for the plasmon response of complex nanostructures*, Science 302 (2003), pp. 419–422.

[70] R. Fernández-García, M. Rahmani, M. Hong, S.A. Maier, and Y. Sonnefraud, *Use of a gold reflecting-layer in optical antenna substrates for increase of photoluminescence enhancement*, Opt. Express 21 (2013), pp. 12552–12561.

[71] P. Benjamin, and C. Weaver, *The adhesion of evaporated metal films on glass*, Proc. R. Soc. London Ser. A 261 (1961), pp. 516–531.

[72] H. Hövel, S. Fritz, A. Hilger, U. Kreibig, and M. Vollmer, *Width of cluster plasmon resonances: Bulk dielectric functions and chemical interface damping*, Phys. Rev. B 48 (1993), pp. 18178–18188.

[73] X. Jiao, J. Goeckeritz, S. Blair, and M. Oldham, *Localization of near-field resonances in bowtie antennae: Influence of adhesion layers*, Plasmonics 4, (2008), pp. 37–50.

[74] B.J. Roxworthy, and K.C. Toussaint, *Plasmonic nanotweezers: strong influence of adhesion layer and nanostructure orientation on trapping performance*, Opt. Express 20 (2012), p. 9591.

[75] J. Kim, K. Cho, and K.S. Lee, *Effect of adhesion layer on the optical scattering properties of plasmonic Au nanodisc*, J. Korean Inst. Met. Mater. 46 (2008), pp. 464–470.

[76] M. Najiminaini, F. Vasefi, B. Kaminska, and J.J.L. Carson, *Optical resonance transmission properties of nano-hole arrays in a gold film: effect of adhesion layer*, Opt. Express 19 (2011), pp. 26186–97.

[77] H. Aouani, J. Wenger, D. Gérard, H. Rigneault, E. Devaux, T.W. Ebbesen, F. Mahdavi, T. Xu, and S. Blair, *Crucial role of the adhesion layer on the plasmonic fluorescence enhancement*, ACS Nano 3 (2009), pp. 2043–2048.

[78] B. Auguié, and W.L. Barnes, *Collective resonances in gold nanoparticle arrays*, Phys. Rev. Lett. 101 (2008), p. 143902.

[79] G. Vecchi, V. Giannini, and J. Gómez Rivas, *Surface modes in plasmonic crystals induced by diffractive coupling of nanoantennas*, Phys. Rev. B 80 (2009), p. 201401.

[80] G. Vecchi, V. Giannini, and J. Gómez Rivas, *Shaping the fluorescent emission by lattice resonances in plasmonic crystals of nanoantennas*, Phys. Rev. Lett. 102 (2009), p. 146807.

[81] B. Ng, S.M. Hanham, V. Giannini, Z.C. Chen, M. Tang, Y.F. Liew, N. Klein, M.H. Hong and S.A. Maier, *Lattice resonances in antenna arrays for liquid sensing in the terahertz regime*, Opt. Express 1(9), (2011), p. 14653.

[82] Y. Chu, E. Schonbrun, T. Yang, and K.B. Crozier, *Experimental observation of narrow surface plasmon resonances in gold nanoparticle arrays*, Appl. Phys. Lett. 9(3), (2008), p. 181108.

[83] A.G. Nikitin, A.V. Kabashin and H. Dallaporta, *Plasmonic resonances in diffractive arrays of gold nanoantennas: near and far field effects*, Opt. Express 20, (2012), pp. 27941–27952.

[84] Y. Chu and K.B. Crozier, *Experimental study of the interaction between localized and propagating surface plasmons*, Opt. Lett. 34, (2009), pp. 244–6.